# Overvoltages Due to Line Faults on a HWL Transmission Line: Corona Effect and Mitigation Techniques

T. M. Pereira, J. S. Acosta, J. A. Santiago, M. C. Tavares

***Abstract*—In half-wavelength (HWL) transmission lines, severe temporary overvoltages are usually observed during the occurrence of line-to-line faults in specific critical locations, and it is unrealistic to ignore the impact of the corona phenomenon. To represent the corona effect, an accurate Suliciu corona model was adopted and implemented in PSCAD software, and a new technique based on the genetic algorithm (GA) was proposed to fit the model parameters. Furthermore, the paper evaluated the performance of the overvoltage mitigation method based on the installation of two spark gaps (SGs) at strategic points to detune the resonance condition. As shown, the SGs turn the HWL line overvoltage levels similar to those observed in conventional AC lines, and the corona modelling further reduces the severity of the overvoltages.**

***Keywords*—half-wavelength transmission lines, corona model, switching overvoltages, fault analysis.**

## I. Introduction

CURRENTLY, bulk power transmission over very long distances is carried out using high-voltage direct current (HVDC) lines. However, a promising alternative to HVDC systems involves transmitting in alternating current (AC) using half-wavelength (HWL) transmission lines. At a 60 Hz power frequency, an HWL line consists of an AC link (point-to-point transmission) with 2600 km in length. The HWL is immune to problems such as the Ferranti effect, excessive load current, and dynamic instability, in addition to presenting a capital expenditure (CapEx) approximately 25% lower than equivalent HVDC [1], [2]. This transmission system has been extensively studied in recent years in countries such as Brazil and China [3]–[9], proving to be a good option for connecting their renewable generating areas to large load centres.

However, an important issue that still needs to be clarified regarding HWL lines is the severe overvoltages that effectively occur in such lines. As noted in previous studies, a native characteristic of HWL lines is the positive sequence resonant condition when three-phase or line-to-line faults occur in specific regions of the line, resulting in severe temporary overvoltages. Although some overvoltage mitigation procedures have been proposed for HWL lines [5]–[9], none of them considered the impact of the corona effect on overvoltages. However, the corona phenomenon acts to dampen the overvoltages, and neglecting its effect can lead to unrealistically overestimated overvoltages [10], [11]. To the best of our knowledge, only the work presented by Illiceto and Cinieri [12] discusses the influence of corona in HWL lines. However, as properly identified by the authors, the corona model adopted was very simplified, incorporating only the corona power losses and being more appropriate for fundamental frequency temporary overvoltage analysis.

Under these circumstances, the most important contribution introduced in the present paper regards the analysis of temporary and switching overvoltages in HWL lines. The corona effect is represented through the accurate Suliciu model [13], [14]. To generate the Suliciu model parameters, a new procedure based on a genetic algorithm is presented, which allows very accurate fitting of the measured charge-voltage ($q - v$) curves. Additionally, the proper representation of the transmission line (TL) response combined with the overvoltage mitigation method based on the installation of SGs reduces the overvoltages to values such as those observed in conventional AC lines. Overall, although the analysis presented is focused on HWL lines, the manuscript contributes to the modelling and simulation of the corona effect for switching and temporary overvoltages in a general way.

The article is organized as follows. Section II describes the system under study. Section III presents the Suliciu corona model and a new procedure to fit its parameters. An analysis and results are presented in Section IV. Finally, Section V presents the main conclusions of the study.

## II. System Under Study

The test system consists of a 735 kV transmission line operating with HWL properties that connects a generating station to a power system (source-grid case), thus constituting a point-to-point transmission. The characteristics of the equivalent systems and TL are described as follows.

### A. Equivalent power systems

The sending station has 4 synchronous machines with step-up transformers (T1), resulting in a three-phase short circuit current (Scc) at the 15 kV busbar of 3.8 kA. The parameters of each machine are based on a real generation

This work was supported in part by the Coordenação de Aperfeiçoamento de Pessoal de Nível Superior - Brasil (CAPES) - Finance Code 001, CNPq (307237 2020 6) and FAPESP (2022/01896-7, 2019/20311-7), Brazil.

Thassio Pereira is with Electrical and Computing Engineering School, University of Campinas, SP, 13083850 Brazil (email:t209420@dac.unicamp.br). Jhair Acosta is with the Electrical and Computing Engineering School, University of Manitoba, Canada (email:jhair.acostasarmiento1@umanitoba.ca). Javier Santiago and Maria Cristina Tavares are with Electrical and Computing Engineering School, University of Campinas, SP, 13083850 Brazil (email:javiersa@dsce.fee.unicamp.br; ctavares@unicamp.br).

Paper submitted to the International Conference on Power Systems Transients (IPST2023) in Thessaloniki, Greece, June 12-15, 2023.

station (Serra da Mesa, Brazil). The receiving system is based on a strong Brazilian 500-kV electrical power system with a Scc off 40 kA (strong point connection). A 735/500 kV step-down transformer (T2) is used to connect the HWL transmission line to the 500 kV power system. In Brazil, the 500 kV network is the most extensive network, and an HWL would be connected to it through a step-down transformer. The power system data are shown in Table I.

TABLE I
POWER SYSTEM PARAMETERS

| Source equivalent impedances | | | | |
|---|---|---|---|---|
| Source | Zero sequence (Ω) | | | |
| Generation – 15 kV | 0.000942 + j 0.032380 | | | |
| Reception system – 500 kV | 7.2169 + j 36.084 | | | |
| Source | Positive/Negative sequences (Ω) | | | |
| Generation – 15 kV | 0.000942 + j 0.032380 | | | |
| Reception system – 500 kV | 0.4801 + j 7.201 | | | |
| Equivalent transformer | | | | |
| Transformer | Xr (%) | kV | MVA | Conection |
| T1 | 11.84 | 735/15 | 2500 | Yn/ Δ |
| T2 | 10.00 | 735/500 | 2500 | Yn/ Yn |

### B. Transmission line

The HWL transmission line adopted in this work consists of a modification of an actual 735 kV Hydro-Quebéc line [15], whose tower geometry is shown in Fig.1. It is worth noting that originally, the 735 kV Hydro-Quebéc line operated in a compensated manner. However, in this work, we adopted the same line geometry, but the length was considered equal to 2600 km so that it could operate with HWL properties. The reason for choosing this line relates to the corona representation implemented in this study. As will be better discussed in Section III, to tune the parameters of the Suliciu corona model, it is necessary to have measurements of $q - v$ curves for the specific conductor bundle of the line. Such measurements are very difficult to find in the literature, especially for cases of dynamic double polarity overvoltages, as occurs during switchings. Fortunately, these measurements were performed for the 4-conductor bundle of the 735 kV Hydro-Quebéc transmission line, as properly described in a 1986 IREQ report [16]. This line has a surge impedance loading (SIL-Pc) of 2038 MW, and the adopted soil resistivity is 2000 Ω.m. Table II shows the electrical parameters for 60 Hz, considering a balanced line.

TABLE II
TRANSMISSION LINE PARAMETERS AT 60 HZ.

| Zero sequence | | |
|---|---|---|
| $R_0(\Omega/km)$ | $X_0(\Omega/km)$ | $B_0(\mu S/km)$ |
| 0.3080 | 1.1060 | 3.4010 |
| Positive/Negative sequences | | |
| $R_1(\Omega/km)$ | $X_1(\Omega/km)$ | $B_1(\mu S/km)$ |
| 0.0111 | 0.3412 | 4.8583 |

## III. CORONA MODELLING

The physical phenomenon of the corona is very complex. It includes ionization, the effects of mobility, diffusion, deionization and the mutual effect of space charges and the electric field [17]. All these phenomena are difficult to separately model for practical applications. For this reason, instead of modelling each microscopic phenomenon separately, the corona models developed for application in EMT-type programs are based on a macroscopic description through charge-voltage (q-v) diagrams, also known as q-v curves (see Fig. 3). In a simple way, the q-v curve relates the conductor voltage to the resulting space charge and synthesizes the main information needed for the representation of the corona effect in transmission lines. The tangent line to the curve is the conductor capacitance, and the area enclosed by the curve is equal to the corona losses. Then, the corona model should properly reproduce the measured q-v curve.

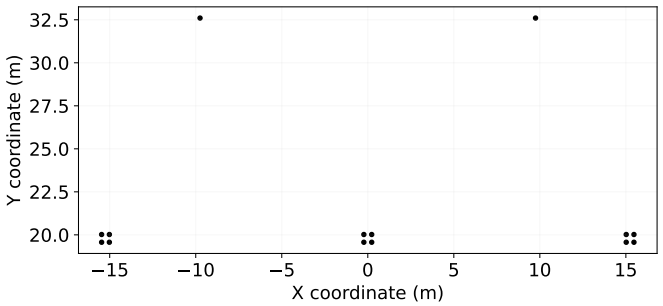


Fig. 1. Tower geometry of the 735 kV Hydro-Quebéc TL (average height of conductors). Bundle is composed of 4 ACSR 3.5 cm diameter conductors spaced 45.70 cm.

In order to perform an accurate representation of the corona phenomenon, the Suliciu corona model is adopted in this work. This model reproduces with good accuracy the characteristics of the measured q-v curves, and is probably the most accurate corona model available for EMT-type applications. This model was initially developed for lightning unipolar overvoltages [18], and it was subsequently extended and applied to switching double-polarity overvoltages [10], [11], [13]. Details about the model are briefly described below, and further information can be found in [19], [14].

### A. Suliciu corona model

If a certain conductor (or conductor bundle) of the transmission line is under corona, air ionization causes the appearance of space charges near its surface, also called corona charges ($Q_c$). Thus, when the conductor voltage becomes zero, part of the charge is attracted to the conductor's surface, and the rest remains concentrated in a cylinder of radius $x$, which can be assumed coaxial to the conductor. In these circumstances, if $C_0$ is the capacitance between the conductor and ground and $C_x$ the capacitance between the conductor and the cylinder surface, it follows that the capacitance between the cylinder surface and the ground ($C_r$) is:

$$C_r = \left(\frac{1}{C_0} - \frac{1}{C_x}\right)^{-1} \tag{1}$$

If V is the voltage between the conductor and the ground, $V_x$ the voltage between the conductor and cylinder surface,

and $Q$ the total charge:

$$V = V_x + \frac{Q}{C_r} \tag{2}$$

$$Q = C_x V_x + Q_c \tag{3}$$

The corona charge $Q_c$ can be obtained by integrating the corona current ($i_c$) inside the cylinder, which by the Suliciu model is obtained as presented in (4).

$$i_c = \frac{d}{dt}Q_c = \begin{cases} 0 & \text{if } g_2 \leq 0 & \text{state 6} \\ g_2 & \text{if } g_1 \leq 0 < g_2 & \text{state 2} \\ g_1 + g_2 & \text{if } g_1 > 0 & \text{state 1} \end{cases} V_x > 0$$
$$\begin{cases} 0 & \text{if } g_4 \geq 0 & \text{state 5} \\ g_4 & \text{if } g_4 < 0 \leq g_3 & \text{state 4} \\ g_3 + g_4 & \text{if } g_3 < 0 & \text{state 3} \end{cases} V_x \leq 0 \tag{4}$$

$$g_m = k_m[(C_m - C_x)(V_x - V_m) - Q_c], \quad m = 1, \ldots, 4 \tag{5}$$

In (4) and (5), $C_m$, $V_m$ and $k_m$ are Suliciu model parameters, which need to be tuned using $q-v$ curves obtained by measurements in corona cages [13], as described in the following section.

### B. Fitting the Suliciu model parameters with a GA

Fig. 2 presents the scheme used to estimate some of the model's parameters when the curve only has positive polarity (unipolar overvoltage). As shown, $C_1$, $C_2$, $V_1$ and $V_2$ can be initially estimated by drawing tangent and secant lines to the measured curve. On the other hand, parameters $k_1$ and $k_2$ can only be obtained through a trial and error approach. The same procedure can be adopted for the case where the voltage has only negative polarity.

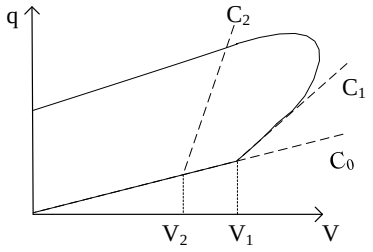


Fig. 2. Estimation of Suliciu model parameters.

However, the difficulty in obtaining the model parameters increases considerably when the $q - v$ curve has a double polarity, which is the case for sustained overvoltages. This is because the values adopted to represent a given half-cycle directly influence the results obtained in the subsequent half-cycle, making it cumbersome to fit the parameters $k_1$, $k_2$, $k_3$ and $k_4$ through trial and error.

To overcome this problem, we fitted the parameters of the Suliciu model through a genetic algorithm (GA) using the objective function in (6), considering that $C_2 > C_1 > C_0$, $C_4 > C_3 > C_0$, $v_1 > v_2 > 0$, $v_3 < v_4 < 0$, and $k_1,\ k_2,\ k_3,\ k_4 > 0$.

$$\min\ f(args) = (q_{real} - q_{fit})^2 + (v_{real} - v_{fit})^2 \tag{6}$$

The GA was set to have a population of 100 individuals, evolving over 100 generations. The crossover probability was set as 90%, and the arithmetic operator was used to generate the offspring. The mutation probability was set to 10%. The amount of mutation was controlled using Gaussian functions with a standard deviation of 100 for $k_m$ and $V_m$ and a standard deviation of 0.1 for $C_m$. Natural selection was performed through modified tournaments using groups with a size of 20% of the total population.

Fig. 3 shows a comparison between the measured $q - v$ curve of the 4-conductor bundle used in the TL described in Section 2 and the curve generated with the Suliciu model using the optimized parameters obtained with the GA, which are presented in Table III. The fitted curve is adherent to the measured data.

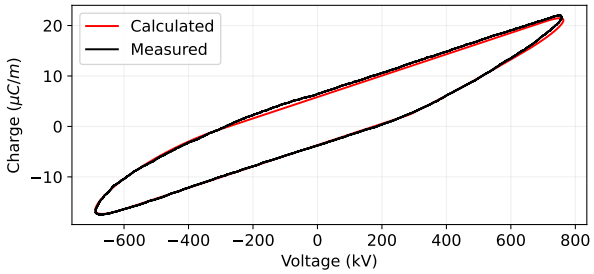


Fig. 3. Measured and calculated $q - v$ curves comparison.

TABLE III
SULICIU MODEL PARAMETERS ADJUSTED THROUGH GAS

| Capacitance values (pF/m) | | | | | |
|---|---|---|---|---|---|
| $C_0$ | $C_1$ | $C_2$ | $C_3$ | $C_4$ | $C_x$ |
| 11.52 | 41.20 | 42.85 | 42.39 | 43.40 | 20.92 |
| k values (Hz) | | | | | |
| | $k_1$ | $k_2$ | $k_3$ | $k_4$ | |
| | 740.59 | 940.27 | 52.24 | 639.22 | |
| Voltage values (kV) | | | | | |
| | $V_1$ | $V_2$ | $V_3$ | $V_4$ | |
| | 797.60 | 400.00 | -594.10 | -443.50 | |

### C. Implementation of the Suliciu model in PSCAD

Equations (1) to (5) are implemented in PSCAD through the *Component Wizard* tool. Then, the Suliciu corona model is represented in the main network by voltage-controlled current sources, wherein the corona current $i_c$ is calculated through the phase-to-ground voltage at each phase of the line. To represent the distributed nature of the corona, the line is discretized into short section lengths, and at each junction node, a shunt corona branch is included (Fig. 4).

## IV. Analysis and Results

To properly evaluate the influence of the corona on the HWL line transient overvoltages, the following modelling and simulation techniques were adopted in PSCAD:

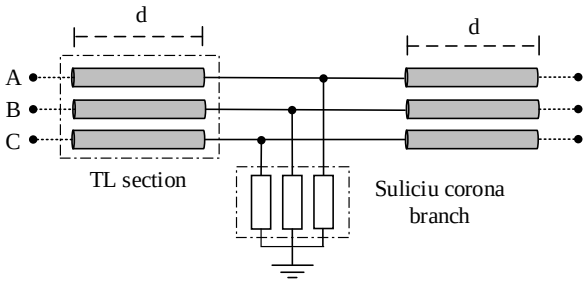


Fig. 4. Implementation of Suliciu corona model in PSCAD.

- The 2600 km HWL line was discretized into 260 sections of 10 km length, and the Suliciu corona branch was connected at each junction node.
- The line was modelled with a phase-domain model (universal line model, ULM) to properly represent the frequency dependence of the TL series parameters. The ground wires were considered incorporated into the equivalent phase parameters, with no impact on the corona modelling. The line was transposed every 100 km.
- The transformer saturation was modelled with a regular core saturation model available in PSCAD. The data of the transformers at both substations were as follows: knee voltage of 1.15 pu, magnetizing current of 1%, and air-core reactance of 0.169 pu.
- Surge arresters (SAs) were connected at the terminal substations, with a reference voltage of 600.12 kV (phase-to-ground). The V-I characteristics were properly represented. A commercial energy absorption rate of 16 kJ/kV was considered, resulting in a maximum absorption capability of 9.6 MV for the nominal voltage of 600.12 kV.
- Typical values of fault resistance were adopted. The three-phase (ABC), three-phase to ground (ABCG), line-to-line (AB - LL) and line-to-line to ground (ABG - LLG) faults were represented by a 10 Ω resistance. Line-to-ground faults (AG, BG, CG - LG) were represented by a 20 Ω resistance [5], [20]. Each fault type was applied at every 50 km of the line, and the phase to ground voltage of each phase was monitored along the entire line.
- For all analyzed cases, the line was in a normal operation condition with nominal loading (1 SIL) at the sending station, and the protection system tripped the line 100 ms after fault occurrence. All fault types were applied at the same instant, namely, at 1.05 s. In addition to fault analysis, the influence of the corona effect on line energization and load rejection manoeuvres was also evaluated.
- To evaluate the influence of the corona effect on the resonant overvoltages, the simulations were initially performed without SGs. An SG is a typical surge protection device with an open-air or enclosed gap used to control overvoltages in HWL lines. Simulations with corona and SGs are explored in the section IV.B, where the spark gap settings are properly explored.

Applying the modelling techniques described above, simulations were performed with and without the corona representation, totalling more than 1500 cases. The main results are summarized and discussed as follows.

### *A. Critical overvoltages*

As demonstrated in [5], the most severe overvoltages in an HWL line are observed when three-phase faults (involving a positive sequence mode) occur around 85% of the line length, as seen by each terminal, resulting in a series resonant condition. To evaluate the influence of the corona effect on these resonant overvoltages, the heatmaps shown in Fig. 5 synthesize the overvoltages that resulted from the application of ABCG faults along the entire line, considering and disregarding the corona effect in the simulations. The maximum overvoltages are marked in the blue dots, and the values are as noted (measured point, fault location). An example of the resulting waveforms for a fault in the resonant region is presented in Fig. 6.

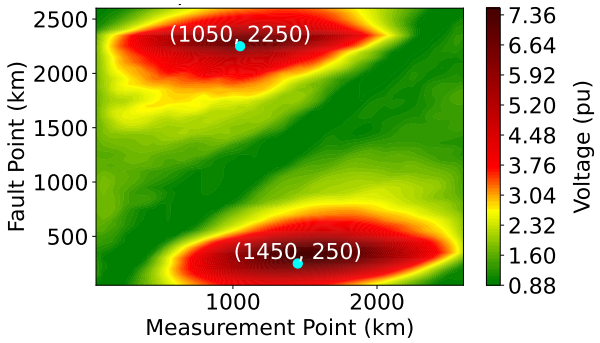


(a) Without corona.

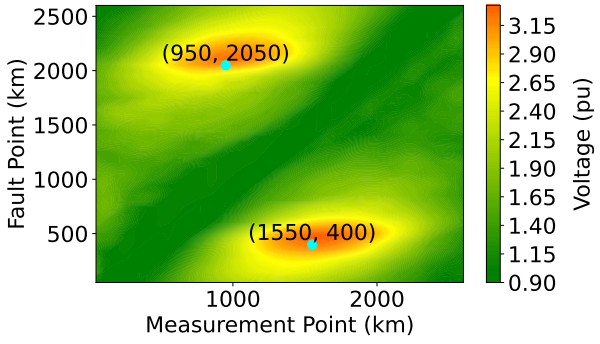


(b) With corona.

Fig. 5. Maximum overvoltages profile in the HWL line under ABCG fault. (a) Simulations without corona representation, (b) Simulations with corona representation.

As seen in the heatmaps and in Fig. 6, not representing the corona phenomenon leads to unrealistic overvoltages for resonant faults, including values higher than 7 pu in the central region of the line. In fact, such high overvoltages are just simulation results produced by the line model adopted and will not occur in the field since multiple flashovers will occur for overvoltages above 3 pu. By representing the corona effect, we can see drastic reductions in the simulation overvoltages. Although resonant faults still occur in the HWL lines, the

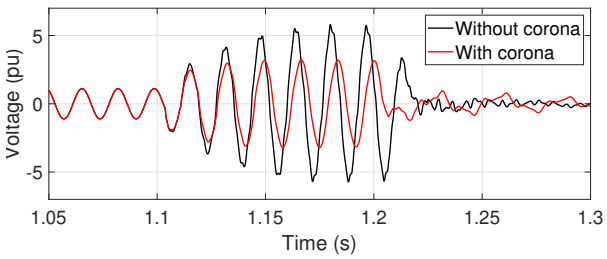


Fig. 6. Voltage at phase A measured at 1000 km - ABCG fault at 2150 km (critical region).

measured overvoltages are below 3.3 pu. These results indicate that, for the analysis of overvoltages caused by resonant faults in the HWL lines, the corona phenomenon cannot be neglected.

The results presented in Fig. 5 also lead to another interesting observation: in addition to drastically reducing the maximum overvoltages, the corona effect causes a displacement of the resonant fault location. As highlighted in the heatmaps, when disregarding the corona effect, the two resonant critical points occur at approximately 250 km and 2250 km, resulting in severe overvoltages at approximately 1450 km and 1050 km, respectively. However, when the corona effect is represented, the critical points are at 400 km and 2050 km, and the most severe overvoltages are observed at 1550 km and 950 km, respectively.

To explain the displacement in the critical fault locations caused by the corona phenomenon, we can observe the wavelength equation of a lossless transmission line in (7).

$$\lambda = \frac{1}{f\sqrt{LC}} \tag{7}$$

where $f$ is the fundamental frequency, and $\lambda$ , $L$ and $C$ are the component sequence wavelength and inductance/capacitance per unit length of transmission line, respectively.

When overvoltages during resonant ABCG faults provoke the corona effect, the equivalent phase capacitance increases as a response to the enlargement of each conductor radius (air ionization). According to (7), the positive sequence wavelength decreases when the capacitance increases, and the critical fault location that is associated with the positive sequence wavelength moves towards the centre of the line. The same result occurs with the associated maximum overvoltage point that is pulled towards its own terminal.

Therefore, in addition to obtaining the appropriate overvoltage level, modelling the corona phenomenon allows the identification of the critical fault region and the associated critical overvoltage locations. It should be noted that if a simplified corona losses model was adopted (as in [12]), the displacement of the critical resonant fault location would not be observed, as in that case, no capacitive corona current was considered.

Although the worst overvoltages occur for three-phase faults, severe overvoltages are also observed for LG and LL faults, and again, the inclusion of the corona effect reduces these overvoltages. Fig. 7 summarizes the maximum overvoltages that were measured along the line for each fault type, with and without corona representation. At each point of measure shown in the graphs, we plot the greatest phase-to-ground voltage obtained between the three phases of the line. Other regular switchings, such as line energization and load rejection, are presented in the figure. For energization, a preinsertion resistor of 300 Ω was adopted, and the results were derived from a statistical simulation with 100 shots and a 2-ms standard deviation for the circuit-breaker pole deviation, considering 20 ms for the main circuit-breaker bypass [5]. For load rejection, we consider the tripping of the nominal loading (1.0 SIL) at 0.5 s.

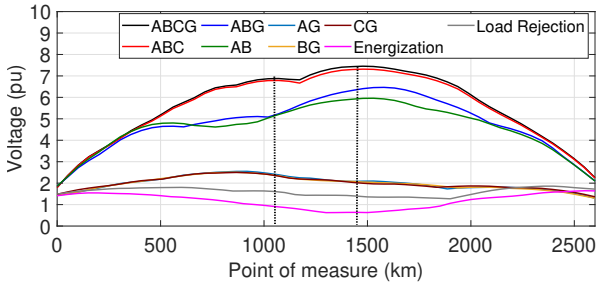


(a) Without corona.

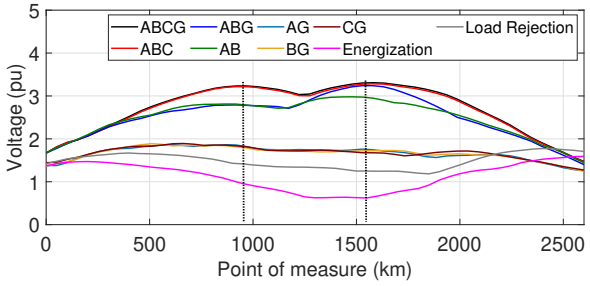


(b) With corona.

Fig. 7. Maximum overvoltage profile along the HWL line for all fault types, line energization, and load rejection. (a) Simulations without corona representation, (b) Simulations with corona representation. Dotted lines highlight the maximum overvoltage points for three-phase faults.

Comparing the results presented in Fig. 7(a) and (b), it can be observed that the corona plays an important role in damping the overvoltages caused by LG and LL faults. Furthermore, the presented results allow the following observations:

- With or without corona representation, the maximum overvoltages provoked by three-phase (ABC) and three-phase-to-ground (ABCG) faults are very similar. Corona modelling reduces overvoltages caused by such faults by approximately 50%. Likewise, the profiles of maximum overvoltages caused by LG faults (AG, BG, and CG) are very similar. The corona effect reduces the maximum overvoltage from 2.55 pu to 1.89 pu (reduction of 26%).
- Line-to-line (AB) and line-to-line to ground (ABG) faults present some differences in the maximum overvoltage profiles. Similar to symmetric faults, LL faults also cause a resonance condition at specific fault locations [4]. Corona modelling reduces the maximum overvoltages caused by this type of fault by approximately 50%.

- Line energization and load rejection present lower overvoltages in most of the line. For these manoeuvres, the corona representation has a smaller influence, reducing the maximum overvoltages by approximately 7%.

### B. Spark Gaps Settings

The results presented in Fig. 7 show that even with corona representation, the overvoltages obtained for resonant faults are considerably high (greater than 3.4 pu). This requires the adoption of techniques to mitigate these severe overvoltages (detune resonance). As demonstrated in [5], an effective way to detune the resonant fault condition is through the installation of two SGs at key points of the line, wherein the highest overvoltages occur. As previously mentioned, an SG is a typical surge protection device with an open-air or enclosed gap used to control overvoltages. The following criteria must be used for locating and designing SGs:

- SGs should coordinate with line-to-ground faults and typical switching (they must only operate for resonant faults).
- SGs must be installed at the two points of the line where the highest overvoltages occur.

As demonstrated in the previous section, the corona effect provokes a displacement of the maximum overvoltage points. This means that the optimal locations of the SGs also change, as shown in the dotted lines of Fig. 7. According to [5], installing SGs at the maximum overvoltage points is important to guarantee their prompt operation and avoid large overvoltages in the system.

Based on the simulation results obtained with and without corona representation, the optimal location ($l$) and voltage breakdown ($V_{BD}$) of each SG are summarized in Table IV. As in [5], the voltage breakdown of each SG is dimensioned considering the maximum overvoltages caused by LG faults at the SG installation point and applying a safety margin of 10%. This ensures that the SG will operate only for resonant faults.

TABLE IV
OPTIMAL GAP LOCATION

| | Without corona | | With corona | |
|---|---|---|---|---|
| | $l$ [km] | $V_{BD}$ [pu] | $l$ [km] | $V_{BD}$ [pu] |
| SG1 | 1050 | 2.63 | 950 | 2.04 |
| SG2 | 1450 | 2.30 | 1550 | 1.92 |

As seen in Table IV, only when the corona phenomenon is modelled is the correct SGs location obtained. Additionally, the devices will operate at much lower voltage values.

### C. Simulations with complete system

The test system is modelled considering the SGs. For simplicity, the analysis presented here refers to a three-phase fault (ABCG) only, as it is the most severe. The SG model used is based on a long electric arc model in free space [21] that can be represented by a primary arc model due to the long electrode distance. The arc voltage model is a voltage source dependent on the arc current. The arc length was considered constant due to the high current level [22].

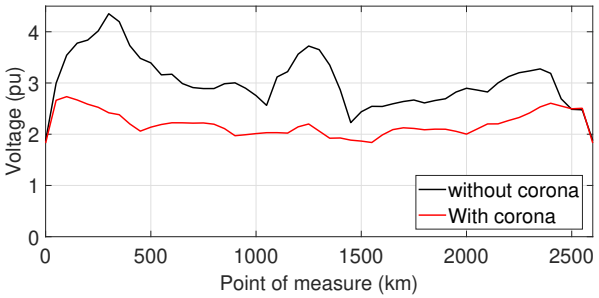


Fig. 8. Maximum overvoltages profile in the HWL line under ABCG fault with SGs.

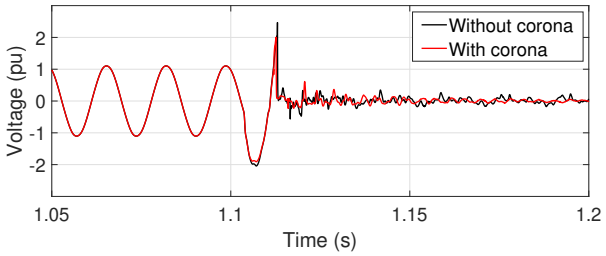


(a) 1000 km.

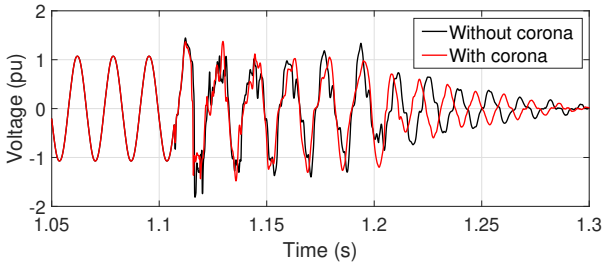


(b) Sending station (0 km)

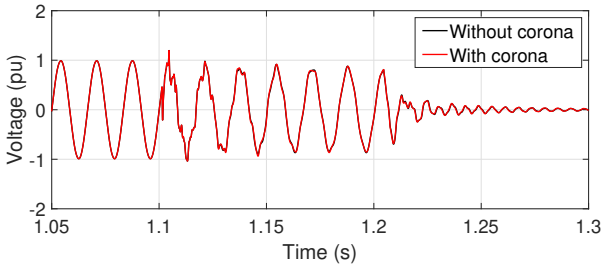


(c) Receiving station (2600 km)

Fig. 9. Voltage at phase A for ABCG fault applied at 2150 km (critical point).

The maximum overvoltage profiles are shown in Fig. 8. The impact of the corona representation can be clearly understood. The overvoltages along the HWL transmission line are no longer extreme; they are similar to those observed in regular length lines. Fig. 9 shows the voltage waveform at phase A in three locations (at 1000 km and line terminals) when the ABCG fault occurs at 2150 km (critical region for the case with and without corona representation – resonance associated with sending terminal). As seen in Fig. 9a, SG1 operates for both cases almost at the same instant, the difference being caused by the breakdown setup value. The corona case produces damped overvoltages at the sending station,

which will have an impact on the surge arresters' energy consumption. No important overvoltage is experienced at the receiving station, as this fault location provokes no overvoltage for the receiving terminal but just for the sending terminal.

Fig. 10 shows the maximum energy absorbed at the sending station (SS) and receiving station (RS) surge arresters for the occurrence of ABCG faults over the entire line. The case without corona representation shows energy levels at the sending station above 10 MJ, while in the corona case, the maximum energy level is reduced to values below 5 MJ.

The presented results show that SGs make the overvoltages in an HWL very similar to those observed in AC lines with conventional lengths. Additionally, the importance of properly representing the corona effect is highlighted, as it further reduces the simulated overvoltage, bringing them to more real values. Thus, unlike some proposals presented in the literature that indicated that HWL SAs should have a larger energy absorption capacity [7], the results presented here indicate that conventional SAs can be installed in HWL lines, resulting in a project cost reduction and reinforcing the feasibility of HWL lines.

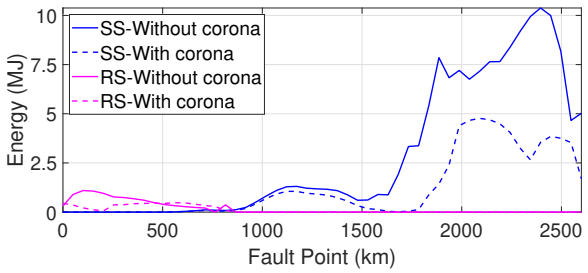


Fig. 10. Surge arresters energy for ABCG faults along the line.

## V. Conclusions

In this work, we assess the influence of the corona effect on the overvoltages of the HWL line, and contributions to the analysis and modelling of the corona for dynamic overvoltages are presented in a general way.

The main conclusions of the paper can be summarized as follows.

- A new scheme based on the use of genetic algorithms is proposed to fit Suliciu's corona model parameters. The use of GA automates the $q - v$ curve fitting process, in addition to ensuring high precision adjustments.
- The corona phenomenon causes displacement of the HWL line critical resonant fault location, which further modifies the points where the maximum overvoltages occur and the associated optimal location of SGs. It was demonstrated that this displacement occurs due to the increase in the shunt capacitive line current caused by the corona phenomenon.
- As previously presented, the SGs are embedded devices of the HWL lines as they remove the resonance fault conditions. However, representing the corona effect further reduces the overvoltages, resulting in a regular energy level of the surge arresters located at terminal substations, such as those observed in AC lines with conventional lengths.

It is important to note that although the analysis carried out in the present study is focused on an HWL system, the results obtained reinforce the importance of properly representing the corona effect for temporary or switching overvoltages. In fact, although there are many references that investigate the influence of the corona on lightning overvoltages, few works deal with temporary or switching overvoltages. The present work intends to fill this gap.

## References

[1] C. Portela, J. Silva, and M. Alvim, "Non-conventional AC solutions adequate for very long distance transmission - An alternative for the Amazon transmission system," *IEC/CIGRE UHV Symposium Beijing*, 2007.

[2] G. Samorodov, S. Kandakov, S. Zilberman, T. Krasilnikova, M. C. Tavares, C. Machado, and Q. Li, "Technical and economic comparison between direct current and half-wavelength transmission systems for very long distances," *IET Generation, Transmission & Distribution*, vol. 11, no. 11, pp. 2871–2878, aug 2017.

[3] F. V. Lopes, B. F. Küsel, K. M. Silva, D. Fernandes, and W. L. Neves, "Fault location on transmission lines little longer than half-wavelength," *Electric Power Systems Research*, vol. 114, pp. 101–109, sep 2014.

[4] J. Santiago and M. C. Tavares, "Relevant factors for temporary overvoltages due to fault-resonance conditions on half-wavelength transmission lines," *Electric Power Systems Research*, vol. 175, no. April, p. 12, 2019.

[5] J. S. Ortega and M. C. Tavares, "Transient Analysis and Mitigation of Resonant Faults on Half-Wavelength Transmission Lines," *IEEE Transactions on Power Delivery*, vol. PP, no. code 001, pp. 1–1, 2019.

[6] H. Tian, H. Liu, H. Ma, P. Zhang, X. Qin, and C. Ma, "Steady-state voltage-control method considering large-scale wind-power transmission using half-wavelength transmission lines," *Global Energy Interconnection*, vol. 4, no. 3, pp. 239–250, jun 2021.

[7] J. Wei, Q. Lu, Z. Le, L. Canbing, and X. Yongwei, "Study on Application of Metal Oxide Arresters for Transient Overvoltage Suppression in the Half-Wavelength Transmission System," in *2017 International Conference on Smart Grid and Electrical Automation (ICSGEA)*, vol. 2017-Janua. IEEE, may 2017, pp. 139–142.

[8] Y. Zhang, Y. Wang, B. Han, L. Ban, Z. Xiang, R. Song, and X. Qin, "Mechanism and mitigation of power fluctuation overvoltage for ultrahigh voltage half-wave length transmission system," *IEEE Transactions on Power Delivery*, vol. 33, pp. 1369–1377, 6 2018.

[9] F. P. Albuquerque, R. F. R. Pereira, E. C. M. Costa, and L. H. B. Liboni, "Temporary overvoltage suppression in half-wavelength transmission lines during asymmetric faults," *Electric Power Systems Research*, vol. 178, p. 106028, 1 2020.

[10] P. S. Maruvada, D. H. Nguyen, and H. Hamadani-Zadeh, "Studies on modeling corona attenuation of dynamic overvoltages," *IEEE Transactions on Power Delivery*, vol. 4, no. 2, pp. 1441–1449, 1989.

[11] M. Cervantes, A. Ametani, C. Martin, I. Kocar, A. Montenegro, D. Goldsworthy, T. Tobin, J. Mahseredjian, R. Ramos, J. Marti, and T. Noda, "Simulation of Switching Overvoltages and Validation With Field Tests," *IEEE Transactions on Power Delivery*, vol. 33, pp. 2884–2893, 12 2018.

[12] F. Iliceto and E. Cinieri, "Analysis of half-wavelength transmission lines with simulation of corona losses," *IEEE Transactions on Power Delivery*, vol. 3, no. 4, pp. 2081–2091, 1988.

[13] H. Hamadani-Zadeh, "Dynamic Corona model and frequency dependent line model for EMTP (IREQ report - Institut de recherche d'Hydro-Québec)," IREQ Report, Tech. Rep., 1986.

[14] J. Mahseredjian, "Corona model - EMTP-RV User's Guide," 2016.

[15] N. G. Trinh, P. S. Maruvada, J. F. Amand, and J. R. Valotaire, "A Study of the Corona Performance of Hydro-Québec's 735-kV Lines," *IEEE Transactions on Power Apparatus and Systems*, vol. PAS-101, pp. 681–690, 3 1982.

[16] P. S. Maruvada and D. H. Nguyen, "Modèle Numerique et Analogique de l'Effet Couronne Utilisé pour le Calcul Surtensions Temporaires - IREQ Internal Report No. IREQ - 5RT3571 G," 1986.

[17] C. de Jesus and M. Correia de Barros, "Modelling of corona dynamics for surge propagation studies," *IEEE Transactions on Power Delivery*, vol. 9, no. 3, pp. 1564–1569, 1994.

[18] M. Mihăilescu-Suliciu and I. Suliciu, "A rate type constitutive equation for the description of the corona effect," *IEEE Transactions on Power Apparatus and Systems*, vol. PAS-100, no. 8, pp. 3681–3685, 1981.

[19] T. M. Pereira, R. Alipio, and M. C. Tavares, "Analysis of Overvoltages Across Line Insulator Strings Considering the Ground-Wire and Phase Conductors Corona," in *Submitted to International Conference of Power System Transients (IPST 2023)*, Thessaloniki, Greece, 2023.

[20] V. D. Andrade and E. Sorrentino, "Typical expected values of the fault resistance in power systems," in *2010 IEEE/PES Transmission and Distribution Conference and Exposition: Latin America (T&D-LA)*, 2010, pp. 602–609.

[21] V. Terzija and H.-J. Koglin, "On the modeling of long arc in still air and arc resistance calculation," *IEEE Transactions on Power Delivery*, vol. 19, no. 3, pp. 1012–1017, 2004.

[22] M. Tavares, J. Talaisys, C. Portela, and A. Camara, "Harmonic content and estimation of length variation of artificially generated electrical arc in out-door experiments," in *2011 IEEE Electrical Power and Energy Conference*, 2011, pp. 346–351.